A microstructural cluster-based description of diffuse and localized failures

N. Hadda
Department of Civil Engineering, University of Calgary, Calgary, Canada

F. Bourrier
Geomechanics Group, ETNA, Irstea, Grenoble, France

L. Sibille
Laboratoire Sols Solides Structures Risques, UJF-INPG-CNRS, Grenoble, France

F. Nicot
Geomechanics Group, ETNA, Irstea, Grenoble, France

R. Wan
Department of Civil Engineering, University of Calgary, Calgary, Canada

F. Darve
Laboratoire Sols Solides Structures Risques, UJF-INPG-CNRS, Grenoble, France

ABSTRACT: This paper presents the analysis of microstructural mechanisms observed during both localized and diffuse failures in granular media, highlighting similarities and differences in their characteristics. Two-dimensional DEM (Discrete Element Method) granular assemblies with medium dense and dense packings were subjected to different biaxial loading paths to induce either a localized or diffuse failure mode. A cluster based analysis is proposed to investigate interactions of particles at the mesoscale through the calculation of the second-order work from microscopic variables. It is shown that such analysis of clusters together with second order work facilitates precise shear band pattern recognition during localized failure. The evolution of such clusters in terms of their spatial distribution, size and number of particles involved, as well as the role played by strong and weak phases, describes the nature of the failure at every stage during loading. Such microstructural descriptors can predict the propensity of the specimen to fail either according to a diffuse or a localized mode.

1 INTRODUCTION

The identification of the underlying micromechanics of failure processes in granular media remains elusive despite numerous studies on the various factors leading to failure. Failure has always been related to either an instability criterion such as the vanishing of the second order work (Hill 1958) or associated with contact networks (Radjai et al. 1999, Iwashita and Oda 2000) namely strong and weak phases, connectivity, cycles and force chain networks (Tordesillas et al. 2010), force chain buckling (Tordesillas 2007) and inter-particles relative motions (Kuhn & Bagi 2004).

Recently, it was shown (Nicot et al. 2012) that the genesis of failure in an assembly of particles is closely related to the sign of the second order work at contacts and its spatial evolution during loading history (Hadda et al. 2013). For instance, based on directional analyses (Gudehus 1979) performed on a dense and loose DEM specimens, it was found that the macroscopic second order work is in good agreement with the second order work computed from microscopic variables. Furthermore, the same study revealed that local instabilities within a granular assembly described by negative or zero values of the second order work at the contact level are in line with the vanishing of the macroscopic second order work. This finding was obtained from some statistical analyses focusing on the population and the spatial distribution of contacts exhibiting negative values of second order work, herein denoted c^-, along all strain probe directions, including those which were proven to be unstable.

For instance, the spatial distribution of c^- contacts is closely related to the emergence of the failure mode, i.e. diffuse and localized. As such, it seems that the understanding of failure process and the triggering of modes is closely associated with how disperse or concentrated the spatial distribution of c^- contacts is. The concentration of c^- contacts conveys the notion of proximity between unstable particles and in the limit refers to finding the most loaded particles with the most c^- contacts. Hence the notion of local instability is most suitably pursued by calculating the sum of second order work at all c^- contacts for a given particle.

Table 1. Physical and mechanical parameters of both specimens S_1 (dense) and S_2 (medium dense).

	S_1	S_2	Unit
Particles diameter range	6–18		mm
Density (ρ)	3,000		kg/m^3
k_n/D(*)	356		(MPa)
k_t/k_n	0.42		–
μ	0.7		–
$\kappa = \frac{k_n}{p}$(**) ($p = 300$ kPa)	1,200		–
Height / Width	1.85	1.35	–
Void ratio (e)	0.174	0.217	–
Coordination number (z)	4.20	3.36	–

*D denotes the mean diameter between two particles in contact.
**κ and p denote respectively the normalized contact stiffness and the mean pressure.

In this paper, and in continuity with our previous studies, the agreement between microscopic and macroscopic second order works is briefly reviewed along a drained biaxial compression. Then, attention is focused on the extent to which c^- contacts relate to the observed failure mode, namely localized and diffuse. Finally, a cluster based approach is introduced in order to highlight the key role of c^- contacts in describing failure at the mesoscale through an aggregation phenomenon.

2 FAILURE MODE ALONG DIFFERENT LOADING PATHS

2.1 *Numerical model*

It is well recognized that the failure mode depends essentially on the density of the granular packing and may be influenced by the loading direction. Thus, in order to achieve distinct failure modes through numerical simulations, two specimens S_1 (dense) and S_2 (medium dense) were considered and each was subjected to a different loading in order to undergo a localized and a diffuse failure respectively.

Both specimens S_1 and S_2 originate from the same two-dimensional discrete element model (Cundall & Strack 1979) consisting of 21,000 particles and they differ only in their initial density (packing). The interparticle interaction is governed by a cohesionless contact law and involves three mechanical parameters: the normal contact stiffness k_n, the tangential contact stiffness k_t and the friction coefficient μ incorporated at the contact level through the Coulomb friction law. The characteristics and mechanical parameters are given in Table 1.

The open source discrete element code Yade (Šmilauer et al. 2010) was used to perform all the simulations presented in this paper.

The granular assemblies were both compacted from an initially sparse cloud of particles to an isotropic state by moving the four rigid frictionless walls toward the center of the specimen until the isotropic pressure

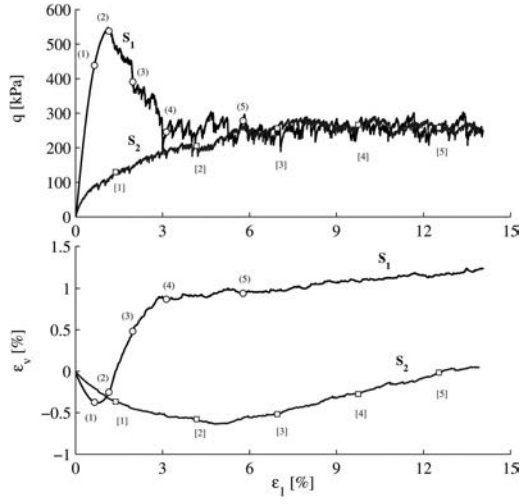

Figure 1. Evolution of the deviatoric stress q and the volumetric strain ε_v in terms of the axial strain ε_1 along the drained biaxial loading performed on S_1 and S_2.

$\sigma_1 = \sigma_2 = 300$ kPa is reached. Both specimens S_1 and S_2 were then subjected to a drained biaxial compression. This compression is carried out by imposing a constant strain rate ($\dot{\varepsilon}_1 = 0.01\ s^{-1}$) as the walls move in the axial direction, and maintaining constant the lateral pressure using a servo-control. In a second simulation, the medium dense specimen S_2 was loaded along a proportional strain path. This type of loading constraints the lateral strain to evolve proportionally to the axial strain at each time step such that $\varepsilon_2 = -\varepsilon_1/R$ (where R is a constant) as walls move in the axial direction at a constant strain rate ($\dot{\varepsilon}_1 = 0.01\ s^{-1}$). Note that for $R < 1$, the loading path is dilatant, for $R > 1$, the loading path is contractant and the case of $R = 1$ coincides with the isochoric loading path. In this study, S_2 was loaded along a dilatant proportional strain path with $R = 0.8$.

The evolutions of the deviatoric stress $q = \sigma_1 - \sigma_2$ and the volumetric strain ε_v in terms of the axial strain ε_1 for S_1 and S_2 resulting from the classic drained compression are plotted in Figure 1. As described, the specimen S_1 shows a typical behavior of a dilatant dense granular medium with a distinctive q peak, while the specimen S_2 exhibits a behavior akin to a medium dense granular medium with a volumetric contractancy up to 5% of axial strain followed by dilatancy.

2.2 *Localized failure*

According to the incremental deviatoric strain $\Delta\varepsilon_{dev}$ fields displayed in Figure 2-a, the dense specimen has clearly underwent a localized failure with a clear shear band after the limit stress state is reached. Incremental volumetric strains, $\Delta\varepsilon_{dev}$, were computed between each successive pair of stress states identified in Figure 1. At the beginning (see snapshot 1), the strain field is

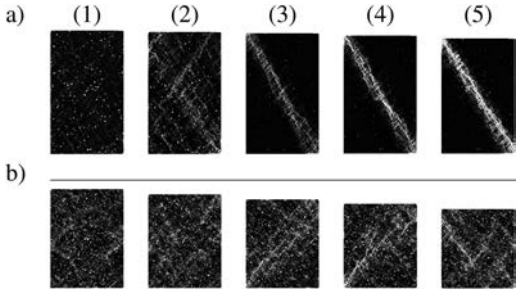

Figure 2. Incremental deviatoric strain fields computed at the stress states 1 to 5 along the drained biaxial compression performed on S_1 (a) and S_2 (b).

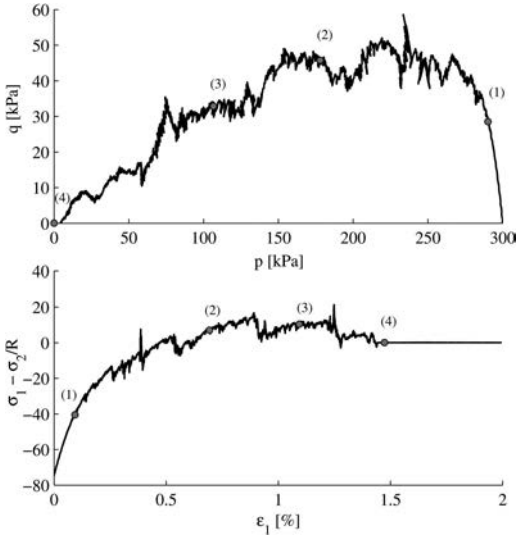

Figure 3. Evolution of the deviatoric stress q and $\sigma_1 - \sigma_2/R$ in terms of the mean pressure p and the axial strain ε_1 respectively along the proportional strain path loading performed on S_2.

homogenous. The snapshot 2 shows not only the fact that strain localizations are well developed at the peak, but also these have already started to define the shear band pattern observed after peak through several thin incipient shear bands. After the peak (see snapshots 3-5), a unique shear band is observed while all others have disappeared. Contrary to what has been observed for S_1, it appears that there is no persistent shear band appearing after failure for the medium dense specimen S_2 as shown in Figure 2-b. However, the incremental deviatoric strain fields computed before peak appear to be similar for both S_1 and S_2 samples.

2.3 *Diffuse failure*

Based on these results reported in the previous section, the medium dense specimen, compared to the dense one, is more susceptible to undergo a diffuse failure along a proportional strain path with a reasonable value of R. Figure 3 shows the evolution of the deviatoric stress q in terms of the mean pressure p. The deviatoric stress q reaches a peak and then both q and p start to decrease until they both vanish. The peak of q for such loading path is not of relevancy when it comes to failure; rather one should consider the peak of $\sigma_1 - \sigma_2/R$ which represent the mixed limit stress state at which the second order work criterion is verified (Nicot et al. 2013). Figure 3 shows that $\sigma_1 - \sigma_2/R$ also passes through a peak, which is slightly exceeded afterward before both σ_1 and σ_2 vanish.

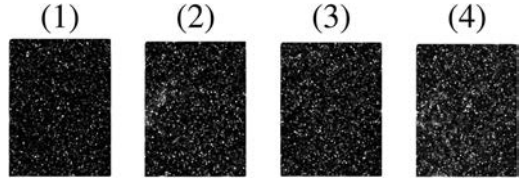

Figure 4. Incremental deviatoric strain fields computed at the stress states 1 to 4 along the proportional strain path loading performed on S_2.

The incremental deviatoric strain fields corresponding to the stress states chosen along the proportional strain path displayed in Figure 4 seem to be quite well homogenous until the vanishing of stresses. Very weak strain localizations can show up intermittently, but they soon fade away. In this case, and on the contrary of what has been observed along the drained compression, the failure is diffuse and develops within the whole granular packing instead of being localized within a shear band.

3 SECOND ORDER WORK FROM MICROSCOPIC VARIABLES

For granular media, it has been shown (Nicot et al. 2012) that the second order work W_2 can be expressed in terms of microscopic variables as:

$$W_2 = \sum_c \Delta \bar{f}^c \Delta \bar{l}^c + \sum_p \Delta \bar{f}^p \Delta \bar{x} \tag{1}$$

The first term of Eq. (1) is a summation over contacts and involves the incremental variations of the contact force $\Delta \bar{f}^c$ and branch vector $\Delta \bar{l}^c$. The second term, a summation over particles, accounts for the inertial effects that may occur during loading. It involves the incremental variation of the resultant force $\Delta \bar{f}^p$ applied on the particle and the variation in position $\Delta \bar{x}$ experienced by the particle during loading.

In the absence of inertial effects (quasi-static regime), which is the case in this study, the contribution of the second term is negligible and W_2 is reduced to:

$$W_2^m = \sum_c \Delta \bar{f}^c \Delta \bar{l}^c \tag{2}$$

First of all, it is interesting to compare the second order work computed from microscopic variable W_2^m with the second order work computed from tensorial

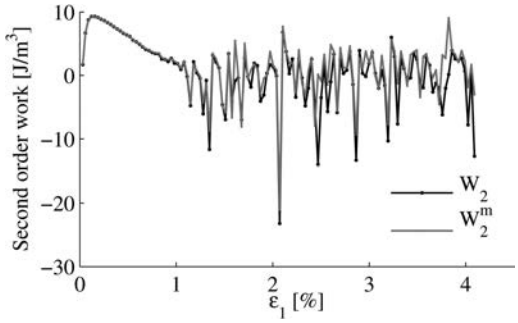

Figure 5. Comparison between the second order works computed from both macroscopic and microscopic variables along the drained compression and the proportional strain loading path performed on S_1 and S_2 respectively.

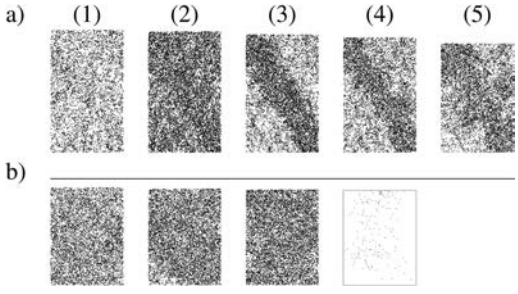

Figure 6. Spatial distributions of c^- contacts computed at the stress states 1 to 5 along the drained compression performed on S_1 (a) and states 1 to 4 along the proportional strain loading path performed on S_2 (b).

variable $W_2 = \Delta\overline{\overline{\sigma}} : \Delta\overline{\overline{\varepsilon}}$ (Nicot et al. 2007), where $\overline{\overline{\sigma}}$ and $\overline{\overline{\varepsilon}}$ are the Cauchy stress tensor and strain tensor respectively, and to see to what extent they are equal along a drained biaxial compression. For this purpose, both second order works were computed between each two successive stress-states chosen at a regular interval along the loading path.

Figure 5 shows that the two second order work expressions, computed differently, agree with each other especially before failure along the classic biaxial compression performed on S_1. The vanishing of the second order work corresponds to the peak of q (i.e. the limit stress state). After failure, a deviation between the two curves may be observed, especially when the specimen undergoes a sharp softening (local avalanche). This phenomenon is usually accompanied by the release of inertial effects, whose contribution may become effective, and thus should be accounted for while computing the second order work from microscopic variables.

This good agreement is confirmed through the spatial distributions of c^- contacts identified at the stress-states 1-5 (Figure 6-a) and 1-4 (Figure 6-b) along the biaxial compression performed on S_1 and the proportional strain path performed on S_2 respectively. Let's recall here that c^- contacts account for those which exhibit a zero or negative value of $w_2 = \Delta\bar{f}^c \Delta\bar{l}^c$. Each c^- contact is presented by a black dot in the snapshots displayed in Figure 6. At the beginning, the spatial distribution of c^- contacts along the biaxial compression is quite homogenous (snapshots 1 and 2). Further c^- contacts become more and more concentrated within the shear band (characterized by the incremental deviatoric strain field) as the axial strain increases. However, the width of the shear band defined by c^- contacts is relatively larger than the one derived from the incremental deviatoric strain field. For the proportional strain loading path, c^- contacts seems to be homogeneously distributed before and after failure with no particular distinguishable structure. Note that in the last snapshot, the sparse number of c^- contacts is due to the loss of contacts within the sample resulting from the static liquefaction, and not to a switch of contacts from negative to positive values of w_2.

The second order work computed from microscopic variables was proven to be in line with the vanishing of the macroscopic second order work. Moreover, the mode of failure can be directly predicted by means of the spatial distribution of c^- contacts. Hence, it definitely constitutes a powerful and suitable tool for the identification of the underlying micro structural mechanisms governing the failure process.

4 CLUSTERS DEFINITION BASED ON $c-$ CONTACTS

Based on the results shown above regarding c^- contacts evolution and distribution during diffuse and localized failures, and according to other findings (Hadda et al. 2013) reporting the strong relation between the increase of c^- contacts number and instability, the distance between c^- contacts seems to play a key role in triggering failure within a granular assembly, especially when the latter come close together. It is definitely clear, that c^- contacts concentrated within the shear band (Figure 6-a) are much closer to each other compared to those outside the band. Moreover, during diffuse failure, the proportional strain loading path seems to prevent c^- contacts from getting much closer, dispersing their concentrations before they get larger. Thus, it is quite interesting to focus the investigations on c^- contacts gatherings for a better understanding of failure triggering and process.

When c^- contacts come so close to each other, this results into another or more contacts belonging to a given particle turning into c^- contacts. Thus, a gathering of c^- contacts can be identified from the most loaded particles and such particles, are most likely to imply

$$\sum_{c \in p} \Delta\bar{f}^c \Delta\bar{l}^c \leq 0 \tag{3}$$

as they sustain more and more c^- contacts.

Regardless of the number of c^- contacts compared to the total number of contacts belonging to a given

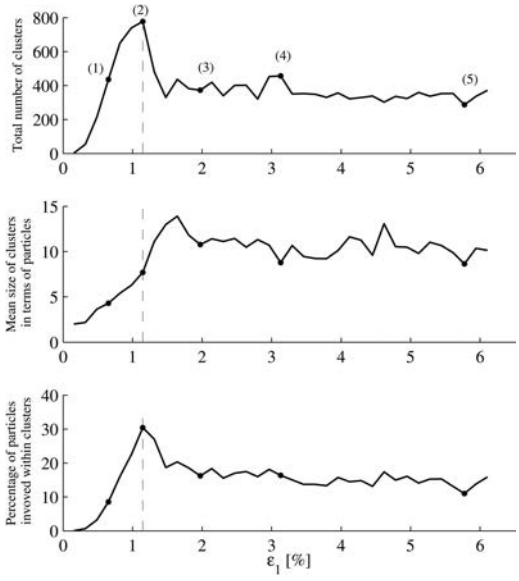

Figure 7. Evolution of the number, mean size of p^- clusters and the number of particles involved within clusters along the drained compression performed on S_1.

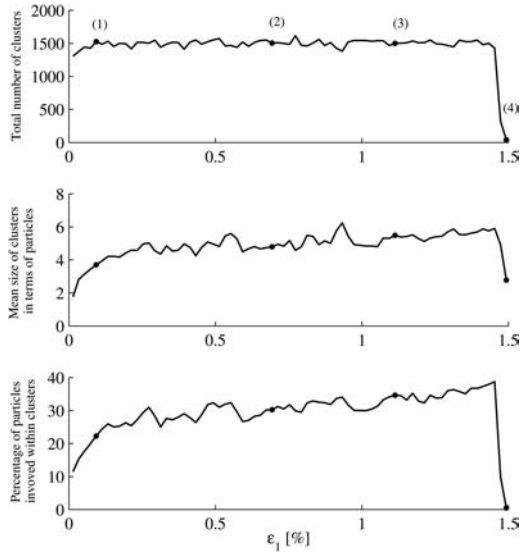

Figure 8. Evolution of the number, mean size of p^- clusters and the number of particles involved within clusters along the proportional loading path performed on S_2.

particle, if the condition (3) is fulfilled, then the particle is likely to be part of a cluster made of at least two particles in contact of that kind. Hence, such particle is denoted by p^-.

In this section, interest will be focused on the evolution and distribution of p^- clusters along both considered loading paths which led to different failure modes.

Figure 7 shows respectively the evolution of the total number, the mean size of p^- clusters and the percentage of particles involved within the clusters for S_1 while undergoing a localized failure. The largest number of clusters formed is reached at the peak of q, involving naturally the largest number of particles. Then, a sharp decrease is observed just after the peak followed by a fluctuation around a constant value.

The ongoing increase of the mean size of p^- clusters during the sharp decrease of the number of clusters right after the peak emphasizes a crucial phase of the localized failure process. This phase corresponds to the appearance of the persistent shear band, throughout which, already existing clusters enlargement and extinction processes take over cluster growth. This result is consistent with what has been observed through the evolution of the incremental deviatoric strain during localized failure (Figure 2-a).

Identically, Figure 8 shows p^- clusters evolution for S_2 while undergoing a diffuse failure. Surprisingly, the evolution of the number of p^- clusters does not show any particular tendency of failure occurrence. In contrast with localized failure, diffuse failure is characterized by an almost constant number of p^- clusters all along the proportional loading path after a rapid modest increase at the beginning of the loading and a spontaneous extinction when static liquefaction fully took place.

Figure 8 shows also a very narrow spread of the mean size of p^- clusters compared to the one observed during the localized failure, which means that p^- clusters formed during such loading preserve almost the same size with a very restricted extension. However, at each peak of $\sigma_1 - \sigma_2/R$, a slight increase of p^- clusters mean size is observed with almost the same number of particles involved within clusters before the peak. Thus, some clusters grow larger during these failure stages but obviously their enlargement is very limited in size and very short in time.

Noticeably, the total number of p^- clusters formed during diffuse failure overwhelm those formed during localized failure and involve more p^- particles. More or less 30% of particles are involved within p^- clusters during diffuse failure while this value is reached only at peak during localized failure and is further reduced to 15%. This phenomenon, which persists during diffuse failure, occurs only at peak during localized failure.

According to Figure 9, where spatial distributions of p^- clusters are displayed at stress states chosen along both loading paths, p^- cluster distribution proves to be more suitable than c^- contacts to directly describe the observed failure mode. For instance, for localized failure, large clusters are found to be distributed within shear bands. Also, the width of the shear band characterized by p^- clusters is not as wide as the one obtained with c^- contact distribution (Figure 6-a), but it rather recalls the one observed in the incremental strain fields (Figure 2-a). Moreover, the p^- cluster spatial distribution was able to point out the slight strain localizations occurring during diffuse failure, which are hardly distinguishable through c^- contact distribution.

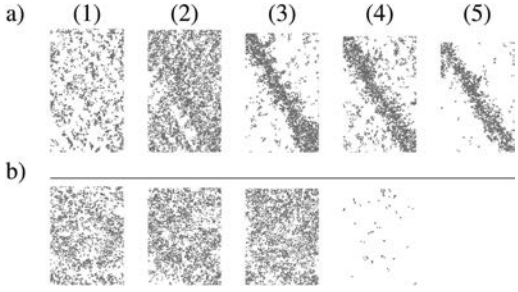

Figure 9. Spatial distribution of p^- clusters at the stress states 1 to 5 along the drained compression performed on S_1 (a) and states 1 to 4 along the proportional strain path loading performed on S_2 (b).

5 CONCLUSIONS

The present study provides a method by which the origins of localized and diffuse failure modes can be deciphered through the analysis of particle clusters in combination with second order work computations. As pointed out in the paper, the DEM studies on both medium dense and dense granular assemblies subjected to biaxial loadings paths lend considerable support to the idea that localization patterns and their evolution are driven inherently by the clustering of particles with contacts violating the second order work. More precisely, the consideration of so-called p^- cluster particles for which the net second order work of all contacting particles is zero or negative leads to a richer interpretation of failure modes, i.e. either localized or diffuse.

REFERENCES

Cundall, P. A. & O. D. L. Strack (1979). A discrete numerical model for granular assemblies. *Geotechnique 29*(1), 47–65.

Gudehus, G. (1979). A comparison of some constitutive laws under radially symmetric loading and unloading. In I. W. Wittke (Ed.), *3rd Int. Conf. Num. Meth. in Geomech.*, A.A. Balkema, Aachen, pp. 1309–1323.

Hadda, N., F. Nicot, F. Bourrier, L. Sibille, F. Radjai, & F. Darve (2013). Micromechanical analysis of second order work in granular media. *Granular Matter*.

Hill, R. (1958). A general theory of uniqueness and stability in elastic-plastic solids. *J. Mech. Phys. Solids 6*, 236–249.

Iwashita, K. & M. Oda (2000, April). Micro-deformation mechanism of shear banding process based on modified distinct element method. *Powder Technology 109*(1–3), 192–205.

Kuhn, M. R. & K. Bagi (2004, October). Contact rolling and deformation in granular media. *International Journal of Solids and Structures 41*(21), 5793–5820.

Nicot, F., A. Daouadji, N. Hadda, M. Jrad, & F. Darve (2013, October). Granular media failure along triaxial proportional strain paths. *European Journal of Environmental and Civil Engineering 17*(9), 777–790.

Nicot, F., F. Darve, & H. D. V. Khoa (2007). Bifurcation and second-order work in geomaterials. *Int. J. Num. Anal. Methods Geomechanics 31*(1007–1032).

Nicot, F., N. Hadda, F. Bourrier, L. Sibille, R. Wan, & F. Darve (2012, May). Inertia effects as a possible missing link between micro and macro second-order work in granular media. *International Journal of Solids and Structures 49*(10), 1252–1258.

Radjai, F., S. Roux, & J. J. Moreau (1999). Contact forces in a granular packing. *CHAOS 9*(3), 544.

Tordesillas, A. (2007). Force chain buckling, unjamming transitions and shear banding in dense granular assemblies. *Philosophical Magazine A – Physics of Condensed Matter Structure Defects & Mechanical Properties. 87*(32), 4987–5016.

Šmilauer, V., E. Catalano, B. Chareyre, S. Dorofeenko, J. Duriez, A. Gladky, J. Kozicki, C. Modenese, L. Scholtès, L. Sibille, J. Stránský, & K. Thoeni (2010). Yade Documentation, The Yade Project.

Tordesillas, A., P. O'Sullivan, & D. M. Walker (2010). Evolution of functional connectivity in contact and force chain networks: Feature vectors, k-cores and minimal cycles. *Comptes Rendus Mécanique 338*(10–11), 556–569.